ChemComm

Accepted Manuscript

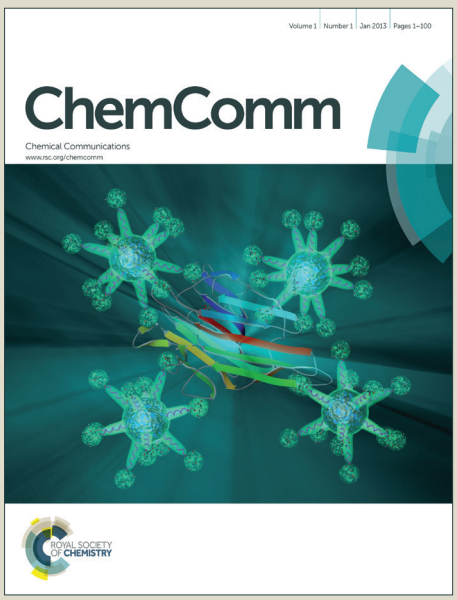

ROYAL SOCIETY OF CHEMISTRY

www.rsc.org/chemcomm

Journal Name

RSCPublishing

COMMUNICATION

Excellent catalytic effects of multi-walled carbon nanotubes supported titania on hydrogen storage of Mg-Ni alloy†

Cite this: DOI: 10.1039/x0xx00000x

Yajun Tan, Yunfeng Zhu, Liquan Li *

Received 00th January 2012,
Accepted 00th January 2012

DOI: 10.1039/x0xx00000x

www.rsc.org/

Superior catalytic effects of multi-walled carbon nanotubes supported titania synthesized by sol–gel method on hydrogen storage of Mg-Ni alloy were investigated. The excellent hydrogen storage properties were obtained: absorbed 5.60 wt.% H_2 within 60 s at 373 K and released 6.08 wt.% H_2 within 600 s at 553 K.

Magnesium hydride has been identified as one of the most attractive materials for hydrogen storage due to its high gravimetric and volumetric hydrogen densities.[1] However, proper strategies are required to overcome the high thermal stability (up to 573 K for hydrogen release) and sluggish sorption kinetics.[2] In the past two decades, many efforts were directed to investigate how to improve the hydrogen storage performance of MgH_2.[3] A commonly successful method is to prepare composite materials by mechanical milling (MM) MgH_2 or Mg with various elements[4] and/or compounds.[5]

It is well known that carbon materials have beneficial effects on the hydrogen sorption of MgH_2. Since the early work of catalyzing MgH_2 with graphite by Imamura et al.,[6] many carbon materials have been extensively studied to promote the hydrogen storage property of MgH_2, including single-walled carbon nanotubes (SWCNTs), multi-walled carbon nanotubes (MWCNTs), carbon nanofibers (CNFs) and activated carbon (AC), as well as graphene nanosheets (GNS).[7] It was found that MWCNTs exhibited the prominent catalytic effect on the hydrogen sorption of MgH_2, not only on improving the de/hydrogenation properties but also on decreasing the starting temperature of the desorption reaction of MgH_2. Previous studies indicate that metal oxides can also have a beneficial effect on the dehydrogenation temperature and kinetics of hydrogen sorption when ball milled with MgH_2. Oelerich et al. investigated the influence of cheap metal oxides on the sorption behaviour of nanocrystalline Mg-based systems.[8] The addition of TiO_2 leads to an enormous catalytic acceleration of hydrogen sorption. Croston et al. investigated the effect of TiO_2 prepared via a sol-gel route, together with the oxide calcination temperature on the H_2 sorption of MgH_2.[9] The results suggest that the anatase form of TiO_2 is more effective at lowering the dehydrogenation onset temperature of MgH_2.

To our knowledge, the TiO_2 is mainly used as a semiconductor photocatalyst.[10] There are no prior studies of the effect of multi-walled carbon nanotubes supported titania (TiO_2/MWCNTs) on improving the properties of MgH_2. In this paper, TiO_2/MWCNTs catalyst was synthesized by sol–gel method followed with calcination. Then, the amount of 5 wt.% TiO_2/MWCNTs was milled with Mg-Ni alloy ($Mg_{95}Ni_5$) synthesized by hydriding combustion synthesis (HCS). The TiO_2 synthesized by sol–gel method and MWCNTs with the same mass percent of 5 wt.% were added separately into $Mg_{95}Ni_5$ for comparison. The XRD patterns of the as-prepared TiO_2/MWCNTs catalyst after drying and heat treatment are shown in Fig. 1. After drying at 353 K, the structure of TiO_2 in TiO_2/MWCNTs is amorphous. Only diffraction peaks of crystalline carbon are observed.

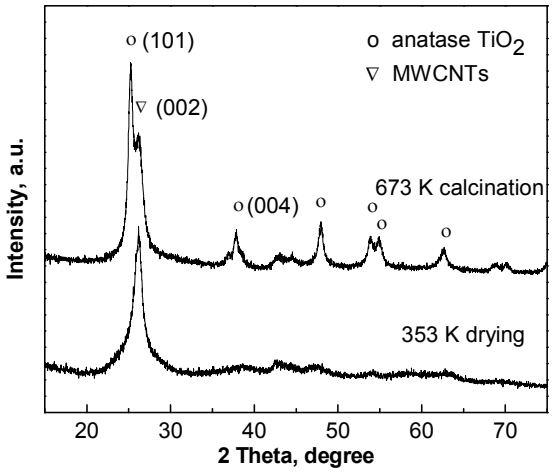

Fig. 1 XRD patterns of the as-prepared TiO_2/MWCNTs catalyst after drying at 353 K and heat treatment at 673 K

However, the anatase structure of TiO_2 appears after calcination at 673 K for 2 h, which is reported more effective at lowering the dehydrogenation onset temperature of MgH_2. Average crystallite size of the anatase phase after calcination at 673 K is 10 nm estimated by Scherrer equation. The XRD pattern of the HCS product of $Mg_{95}Ni_5$ is shown in Fig. S1 (ESI†). The peaks

corresponding to MgH_2, Mg_2NiH_4, $Mg_2NiH_{0.3}$ and un-reacted Mg are detected. Although the hydrogenation degree is not high, the activity of the HCS product of $Mg_{95}Ni_5$ is high, which will be reflected in the following de/hydrogenation process.

The morphology information of the as-prepared TiO_2/MWCNTs is supported by the TEM and high-magnification TEM images shown in Fig. 2. The TEM bright images of TiO_2/MWCNTs under different magnifications show that the diameter of the MWCNTs is about 40 nm. Small nanoparticles with different sizes (about 5-20 nm) exist on the surface of the MWCNTs. Combined with the XRD results of TiO_2/MWCNTs, it can be inferred to be TiO_2 nanoparticles. The HRTEM image in b shows that the lattice fringes with a separation of 0.236 nm agree well with the (004) interplanar spacing of TiO_2; and the lattice fringes with a separation of 0.338 nm agree well with the (002) interplanar spacing of MWCNTs.

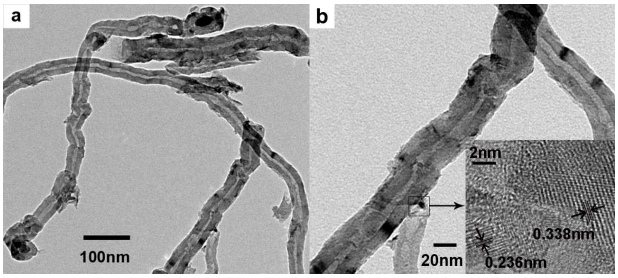

Fig. 2 TEM images of TiO_2/MWCNTs catalyst under different magnifications; the inset in (b) gives the HRTEM image of the selected area

The catalytic effect of TiO_2/MWCNTs on the hydrogen desorption properties of $Mg_{95}Ni_5$ was investigated. Fig. S2 (ESI†) shows the amount of hydrogen desorbed as a function of temperature of the as-milled $Mg_{95}Ni_5$ and $Mg_{95}Ni_5$-TiO_2/MWCNTs. It can be seen that the $Mg_{95}Ni_5$-TiO_2/MWCNTs exhibits the faster dehydriding kinetics, which releases all the hydrogen below 546 K (~ 603 K for $Mg_{95}Ni_5$). Besides, the dehydriding onset temperature (at which hydrogen begin to release) of $Mg_{95}Ni_5$-TiO_2/MWCNTs is decreased from 458 K for $Mg_{95}Ni_5$ to 443 K, which is also much lower than as-milled commercial MgH_2 (~ 573 K).

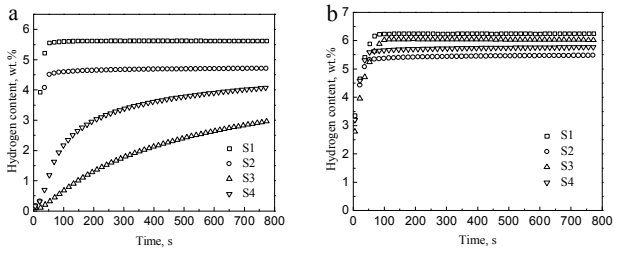

Fig. 3 Isothermal hydrogenation curves of (S1) $Mg_{95}Ni_5$-TiO_2/MWCNTs, (S2) $Mg_{95}Ni_5$-TiO_2, (S3) $Mg_{95}Ni_5$-MWCNTs and (S4) $Mg_{95}Ni_5$ at (a) 373 K and (b) 493 K under 3.0 MPa hydrogen pressure.

The hydrogen absorption curves of the $Mg_{95}Ni_5$-TiO_2/MWCNTs, $Mg_{95}Ni_5$-TiO_2, $Mg_{95}Ni_5$-MWCNTs and $Mg_{95}Ni_5$ at 373 K and 493 K are shown in Fig. 3. It can be noticed that the $Mg_{95}Ni_5$-TiO_2/MWCNTs exhibits drastically fast hydriding rate at 373 K, which reaches its saturated hydrogen absorption capacity of 5.60 wt.% within 60 s. Similarly, $Mg_{95}Ni_5$-TiO_2 also shows fast hydrogen absorption rate under the same condition, absorbing 4.60 wt.% hydrogen within 100 s. However, the $Mg_{95}Ni_5$ absorbs only 4.07 wt.% H_2 at the same temperature. As shown in Fig. 3b, all the samples have drastically fast hydriding rates at 493 K. The $Mg_{95}Ni_5$-TiO_2/MWCNTs absorbs 6.25 wt.% H_2 (theoretical capacity of 6.50 wt.%), which is higher than 5.77 wt.% of $Mg_{95}Ni_5$ (theoretical capacity of 6.85 wt.%). Besides, with the addition of MWCNTs, the saturated hydrogen absorption capacity of $Mg_{95}Ni_5$ is also improved. The hydrogen absorption capacities of all the samples are listed in Table S1 (ESI†). It is revealed that the TiO_2/MWCNTs has the excellent catalytic effects on the hydrogenation, not only can it enhance the kinetics performance, but it can also increase the hydrogen absorption capacity.

To analyse the hydrogen desorption kinetics of $Mg_{95}Ni_5$-TiO_2/MWCNTs, isothermal dehydrogenation measures were performed at different temperatures. Fig. 4 shows the isothermal dehydrogenation curves of the $Mg_{95}Ni_5$-TiO_2/MWCNTs, $Mg_{95}Ni_5$-TiO_2, $Mg_{95}Ni_5$-MWCNTs and $Mg_{95}Ni_5$ at 523 K and 553 K (493 K and 573 K are shown in Fig. S3, ESI†). At 523 K, a hydrogen desorption capacity of 5.95 wt.% can be reached for $Mg_{95}Ni_5$-TiO_2/MWCNTs. However, the $Mg_{95}Ni_5$ releases only 4.47 wt.% H_2 within the same time. Furthermore, at 553 K, the $Mg_{95}Ni_5$-TiO_2/MWCNTs reaches its saturated hydrogen desorption capacity of 6.08 wt.% within 600 s, displaying the excellent kinetics of dehydrogenation. With the addition of TiO_2 alone, the dehydrogenation kinetics of $Mg_{95}Ni_5$ is also improved. Even at the low temperature of 493 K (Fig. S3a, ESI†), the $Mg_{95}Ni_5$-TiO_2/MWCNTs can release 2.24 wt.% H_2, which is three times more than $Mg_{95}Ni_5$ (0.78 wt.%). Thus, the addition of TiO_2/MWCNTs also has the high catalytic effects on the hydrogen desorption of $Mg_{95}Ni_5$. The hydrogen desorption capacities of all the samples are listed in Table S2 (ESI†).

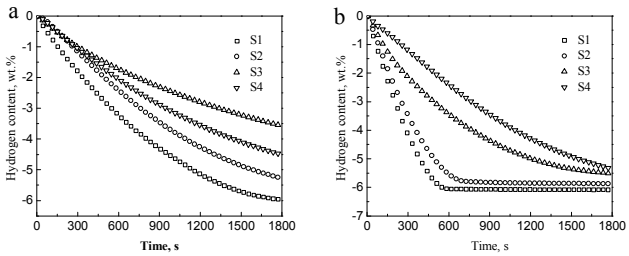

Fig. 4 Isothermal dehydrogenation curves of (S1) $Mg_{95}Ni_5$-TiO_2/MWCNTs, (S2) $Mg_{95}Ni_5$-TiO_2, (S3) $Mg_{95}Ni_5$-MWCNTs and (S4) $Mg_{95}Ni_5$ at (a) 523 K and (b) 553 K under the pressure of 0.005 MPa

To further understand the dehydrogenation kinetics mechanism, the activation energy (E_A) for the dehydrogenation of the MgH_2-TiO_2/MWCNTs was determined by the JMA model and Arrhenius equation after fitting the experimental desorption data. Fig. S4 (ESI†) illustrates the JMA plots of ln [−ln (1−α)] vs ln (t) for the desorption data at different temperatures. The values of the exponent n are in the range of 1.0~1.2, which indicate that the nucleation of Mg occurs quickly and the growth is controlled by one-dimensional diffusion.[11] The Arrhenius plots for the dehydriding kinetics of $Mg_{95}Ni_5$-TiO_2/MWCNTs are shown in Fig. S5 (ESI†). The activation energy E_A for hydrogen desorption of MgH_2 is 79.13 kJ mol^{-1} H_2, which is lower than 153 kJ mol^{-1} H_2 of the as-received commercial MgH_2,[12] thus providing further evidence for the correlation between the presence of TiO_2/MWCNTs and the hydrogen desorption kinetics.

The experimental results have demonstrated that the hydrogen storage properties of $Mg_{95}Ni_5$-TiO_2/MWCNTs are considerably enhanced compared with $Mg_{95}Ni_5$. The TiO_2 nanoparticles distributed on the surface of MWCNTs accelerate de/hydrogenation kinetics, while MWCNTs makes contribution to improve hydrogen absorption/desorption capacity. The enhance mechanism of TiO_2/MWCNTs addition on the hydrogen absorption/desorption performances of $Mg_{95}Ni_5$ are discussed as follows.

First, it should attribute to the relatively high specific surface area of TiO_2/MWCNTs catalyst. The nitrogen adsorption and desorption isotherm curves of the as-prepared TiO_2/MWCNTs are shown in Fig. S6 (ESI†). The Brunauer–Emmett–Teller (BET) specific surface area of TiO_2/MWCNTs catalyst is 87.2 m^2g^{-1}, which is larger than MWCNTs of 40-70 m^2g^{-1} according to the specification. Compared with Nb_2O_5 of 46 m^2g^{-1} and MWCNTs of 47 m^2g^{-1} reported by literatures, it is also larger.[7a, 13] Although the specific surface area of TiO_2/MWCNTs is relatively lower than pure TiO_2 (118.5 m^2g^{-1}), the hydrogen storage properties of $Mg_{95}Ni_5$-TiO_2/MWCNTs are more excellent with the synergetic catalysis of MWCNTs and TiO_2. Because the MWCNTs not only can improve the efficiency of mechanical milling, but it can also make the TiO_2 nanoparticles fully dispersed and facilitate the diffusion of the hydrogen atom. The TiO_2/MWCNTs catalyst with relatively high specific surface area can provide more edge sites, thus providing more channels for hydrogen diffusion.

Second, the $Mg_{95}Ni_5$-TiO_2/MWCNTs has a smaller crystallite size of MgH_2 than the $Mg_{95}Ni_5$, resulting in more fraction of grain boundary, which is helpful to shorten the hydrogen diffusion distances.[14] The XRD patterns of $Mg_{95}Ni_5$ and $Mg_{95}Ni_5$-TiO_2/MWCNTs after mechanical milling are shown in Fig. 5. The average crystallite sizes of MgH_2 phase in the as-milled $Mg_{95}Ni_5$ and $Mg_{95}Ni_5$-TiO_2/MWCNTs were estimated to be 28.9 nm and 14.0 nm, respectively. The SEM images of $Mg_{95}Ni_5$ and $Mg_{95}Ni_5$-TiO_2/MWCNTs after mechanical milling, and the size distribution of the samples are shown in Fig. S7 (ESI†). The average grain size and particle size of MgH_2 are decreased with the addition of TiO_2/MWCNTs, which should enhance Mg-H interface reaction kinetics. The XRD pattern of $Mg_{95}Ni_5$-TiO_2/MWCNTs after dehydrogenation is shown in Fig. S8 (ESI†). Mainly Mg, Mg_2Ni, and MgO were detected, indicating the complete dehydrogenation of $Mg_{95}Ni_5$. The average crystallite size of Mg in $Mg_{95}Ni_5$-TiO_2/MWCNTs after dehydrogenation is 43.6 nm. It is in agreement with other studies that the crystallite size of the composite increases with cycling.

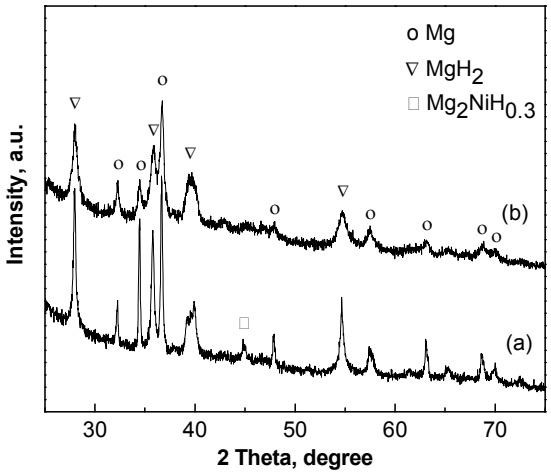

Fig. 5 XRD patterns of (a) $Mg_{95}Ni_5$ and (b) $Mg_{95}Ni_5$-TiO_2/MWCNTs after mechanical milling

As a third possible explanation, the literature reported active metal Ti species could be formed during the processes of milling and dehydrogenation for MgH_2 added with TiO_2.[9,15] The XPS test of $Mg_{95}Ni_5$-TiO_2/MWCNTs after mechanical milling was carried out to examine the nature of the Ti species (Fig. S9, ESI†). Fitting of these peaks shows the characteristic peaks of Ti^{4+} (459.1 eV and 464.8 eV for Ti $2p_{3/2}$ and Ti $2p_{1/2}$ peaks) and Ti (460.1 eV for Ti $2p_{1/2}$ peak), which is in accord with the reference data shown in Table S3 (ESI†).[15,16] It suggests that Ti of a lower oxidation state than +4 can be generated by the high local temperature arising during mechanical milling. The possible chemical reaction in mechanical milling is given below, showing that active metal Ti will generate at the expense of oxidation of Mg.

$$2Mg + TiO_2 = Ti + 2MgO \qquad \Delta G\ (300\ K) = -330\ kJ\ mol^{-1}$$

The energy barrier of the hydrogen dissociation is as high as 4.52 eV, which is impossible to dissociate H_2 to atomic H under normal circumstances. However, the energy barrier of the hydrogen dissociation on Ti-incorporated Mg (0001) surface was calculated to be 0.103 eV, which is much lower than on pure Mg (0001) of 1.05 eV.[17] It means that the existence of Ti could contribute to the dissociation of hydrogen molecules.

In conclusion, multi-walled carbon nanotubes supported titania synthesized by sol–gel method with a relatively high specific surface area of 87.2 m^2g^{-1} had excellent catalytic effects on hydrogen storage of $Mg_{95}Ni_5$. With the addition of TiO_2/MWCNTs catalyst, the $Mg_{95}Ni_5$ absorbed 5.60 wt.% H_2 within 60 s at 373 K and released 6.08 wt.% H_2 within 600 s at 553 K. The superior catalytic effects should be attributed to the grain refinement of $Mg_{95}Ni_5$ and the relatively high specific surface area of TiO_2/MWCNTs catalyst, providing more channels for hydrogen diffusion to enhance the de/hydrogenation kinetics and improve the hydrogen absorption/desorption capacity of $Mg_{95}Ni_5$. Moreover, the generation of active metal Ti derived from TiO_2 could also contribute to the dissociation of hydrogen molecules.

This work was supported by the National Natural Science Foundation of China (NSFC) (Grant Nos. 51471087, 51171079), Natural Science Foundation of the Jiangsu Higher Education Institutions of China (Grant No. 13KJA430003), Innovation Foundation for Graduate Students of Jiangsu Province (Grant No. KYLX_0741, CXZZ13_0420), Qing Lan Project and the Priority Academic Program Development (PAPD) of Jiangsu Higher Education Institutions.

Notes and references

College of Materials Science and Engineering, Nanjing Tech University, 5 Xinmofan Road, Nanjing, 210009, P.R. China.
E-mail: lilq@njtech.edu.cn; Tel: +86-25-83587255

† Electronic Supplementary Information (ESI) available: Experimental Details, Characterization method, Table S1, S2 and S3, Fig. S1~S9 as mentioned in the text. See DOI: 10.1039/c000000x/

1 (a) C. Liu, F. Li, L. P. Ma and H. M. Cheng, *Adv. Mater.*, 2010, **22**, E28-62; (b) G. Liu, F. Y. Qiu, J. Li, Y. J. Wang, L. Li, C. Yan, L. F. Jiao and H. T. Yuan, *Int. J Hydrogen Energy*, 2012, **37**, 17111-17117.

2 F. Y. Cheng, Z. L. Tao, J. Liang and J. Chen, *Chem. Commun.*, 2012, **48**, 7334-7343.

3 (a) M. X. Gao, J. Gu, H. G. Pan, Y. L. Wang, Y. F. Liu, C. Liang and Z. X. Guo, *J. Mater. Chem.*, 2013, **1**, 12285-12292; (b) K-J. Jeon, H. R. Moon, A. M. Ruminski, B. Jiang, C. Kisielowski and R. Bardhan, *Nat. Mater.*, 2011, **10**, 286-290; (c) C. Y. Zhu, S. Hosokai and T. Akiyama, *Cryst. Growth. Des.*, 2011, **11**, 4166-4174.

4 (a) R. R. Shahi, A. P. Tiwari, M. A. Shaz and O. N. Srivastava, *Int. J Hydrogen Energy*, 2013, **38**, 2778-2784; (b) L. Z. Ouyang, Z. J. Cao, H. Wang, J. W. Liu, D. L. Sun, Q. A. Zhang and M. Zhu, *J Alloys Compd.*, 2014, **586**, 113-117; (c) J. Cui, J. W. Liu, H. Wang, L. Z. Ouyang, D. L. Sun, M. Zhu and X. D. Yao, *J. Mater. Chem. A*, 2014, **2**, 9645-9655.

5 (a) C. S. Zhou, Z. Z. Fang, C. Ren, J. Z. Li and J. Lu, *J. Phys. Chem. C*, 2013, **117**, 12973-12980; (b) H. Z. Liu, X. H. Wang, Y. A. Liu, Z. H. Dong, H. W. Ge, S. Q. Li and M. Yan, *J. Phys. Chem. C*, 2014, **118**, 37-45; (c) C. H. An, G. Liu, L. Li, Y. J. Wang, C. C. Chen, Y. J. Wang, L. F. Jiao and H. T. Yuan, *Nanoscale*, 2014, **6**, 3223-3230.

6 (a) H. Imamura, N. Sakasai and T. Fujinaga, *J. Alloys Compd.*, 1997, **253**, 34-37; (b) H. Imamura, Y. Takesue, T. Akimoto and S. Tabata, *J. Alloys Compd.*, 1999, **293-295**, 564-568.

7 (a) M. A. Lillo-Ródenas, Z. X. Guo, K. F. Aguey-Zinsou, D. Cazorla-Amorós and A. Linares-Solano, *Carbon*, 2008, **46**,126-137; (b) B. S. Amirkhiz, M. Danaie, M. Barnes, B. Simard and D. Mitlin, *J. Phys. Chem. C*, 2010, **114**, 3265-3275; (c) Y. Jia, Y. N. Guo, J. Zou and X. D. Yao, *Int. J Hydrogen Energy*, 2012, **37**, 7579-7585; (d) G. Liu, Y. J. Wang, C. C. Xu, F. Y. Qiu, C. H. An, L. Li, L. F. Jiao and H. T. Yuan, *Nanoscale*, 2013, **5**, 1074-1081.

8 W. Oelerich, T. Klassen and R. Bormann, *J. Alloys Compd.*, 2001, **315**, 237-242.

9 D. L. Croston, D. M. Grant and G. S. Walker, *J. Alloys Compd.*, 2010, **492**, 251-258.

10 (a) Y. Y. Liang, H. L. Wang, H. S. Casalongue, Z. Chen and H. J. Dai, *Nano Res*, 2010, **3**, 701-705; (b) S. N. Basahel, K. Lee, R. Hahn, P. Schmuki, S. M. Bawaked and S. A. Al-Thabaiti, *Chem. Commun.*, 2014, **50**, 6123-6125 ; (c) Y. M. Zhu, D. S. Liu and M. Meng, *Chem. Commun.*, 2014, **50**, 6049-6051.

11 (a) Y. P. Pang, Y. F. Liu, X. Zhang, M. X. Gao and H. G. Pan, *Int. J Hydrogen Energy,* 2013, **38**, 1460-1468; (b) C. Y. Zhu and T. Akiyama, *Cryst. Growth Des.*, 2012, **12**, 4043-4052.

12 Y. J. Choi, J. Lu, H. Y. Sohn and Z. Z. Fang, *J. Power Sources*, 2008, **180**, 491-497.

13 V. V. Bhat, A. Rougier, L. Aymard, G. A. Nazri and J. M. Tarascon, *Journal of Alloys and Compounds*, 2008, **460**, 507-512.

14 Y. P. Pang, Y. F. Liu, M. X. Gao, L. Z. Ouyang, J. W. Liu, H. Wang, M. Zhu and H. G. Pan, *Nat. Commun.*, 2014, **5**, 3519-3527.

15 A. Ermolieff, P. Bernard, S. Marthon and P. Wittmer, Surf. Interface Anal., 1988, **11**, 563-568.

16 D. Gonbeau, C. Guimon, G. Pfisterguillouzo, A. Levasseur, G. Meunier and R. Dormoy, Surf. Sci., 1991, **254**, 81-89.

17 A. J. Du, Sean C. Smith, X. D. Yao and G. Q. Lu, *J. Phys. Chem. B*, 2005, **109**, 18037-18041.

